Journal of Thermal Analysis and Calorimetry
https://doi.org/10.1007/s10973-023-11981-0

3D Numerical investigation of flow and heat transfer from an immersed vertical cylinder with the constant rotation speed in an unbounded stationary fluid

Amir Mansourian[1] · **Asghar B. Rahimi**[1]

Received: 3 December 2022 / Accepted: 19 January 2023

Abstract
This paper obtains the rotational speed effects of an immersed rotating vertical cylinder at constant temperatures on convection (heat transfer) within stationary fluids. The finite volume method in accordance with the commercial CFD solver FLUENT is used to solve the main equations. The wall domain effect is also examined by changing the aspect ratio. The results show that the effect of the walls disappears in the aspect ratios of 4 and above. Various Reynolds numbers (Re) (200–3000) are taken into account to perform simulations. The flow and thermal field details are described by exploring variations of flow vector, isothermal contour, iso-surface temperature, local and average Nusselt number (Nu), and velocity components. The results indicate convincing evidence of the strong impact of the increase in rotation speed or Re on the flow patterns and heat transfer. An increase in Re from 200 to 3000 enhances the average Nu by 68%. The laminar-to-turbulent flow changes are reported when Re values are close to 1000. Performance evaluations are carried out for LES and UARNS turbulence methods at Re = 3000 to accurately obtain the simulating vortices and their effect on heat transfer. Based on the findings, only LES could provide an accurate structure for the secondary flows with a significant effect on heat transfer.

Keywords Laminar and turbulent flow · Convective heat transfer · Rotating vertical cylinder · Reynolds number · URANS · LES

List of symbols

a	Inner vertical cylinder diameter (m)
b	Outer vertical cylinder diameter (m)
r, θ, z	Cylindrical coordinate
s	Height of cylinder (m)
Y	Expressing height (m)
V	Velocity (m s^{-1})
T	Temperature (K)
g	Gravitational acceleration (m s^{-2})
h	Heat transfer coefficient (W m^{-2} K^{-1})
k	Thermal conductivity (W m^{-1} K^{-1})
U_0	Reference velocity (m s^{-1})
Pr	Prandtl number
Gr	Grashof number
Nu_{mean}	Average Nusselt number
Nu_{Local}	Local Nusselt number
Re	Reynolds number

Greek symbols

ν	Kinematic viscosity, m^2 s^{-1}
λ	Aspect ratio
w	Angular velocity of cylinder, rad s^{-1}
β	Thermal expansion coefficient, K^{-1}
μ	Dynamic viscosity (N-s m^{-2})
ρ	Density (Kg m^{-3})

Subscript

i	Inner
o	Outer
H	Hot
C	Cold

Introduction

Rotating cylinders have many applications. Rotary fractionation columns can be considered as one of its applications. Many other uses can also be mentioned, for example vortex flow reactor that used for reproducibility and scale-up of chemical reactions. Seafloor process is another application in which the rotating cylinder for investigated dynamics of

✉ Asghar B. Rahimi
rahimiab@yahoo.com

[1] Department of Engineering, Ferdowsi University of Mashhad, Mashhad, Iran

Published online: 03 March 2023

aggregation and algal growth is used. Screw extruders in polymer industries and labyrinth pumps are one of the other uses of the rotating cylinders. So, for a correct understanding of the behavior of the rotating cylinders in each of the mentioned applications and effective design, it is necessary to study the flow and heat transfer. Most of the assumptions for study of the flow have been made with the assumption that the flow is laminar, but the results are far from the reality; therefore in the last decade, the development of new industrial tools was accompanied by considering turbulent flow and heat transfer in preliminary designs. The Reynolds averaged Navier–Stokes (RANS) relations were used to predict turbulent flows [1–5]. The large eddy simulation (LES) methodology offers better results when more precise details of the turbulent flow are required, although this method has more computational costs [6–10]. Mixed convection may occur in many industrial applications and natural phenomena. The flow passing a vertical rotating cylinder or a rotating cylinder in a stationary fluid is some of these applications which were widely examined. Concerning the motion of circular cylinders in a viscous fluid, Frazer [11] theoretically solved two-dimensional problems for a fluid bounded by circular cylinders. Riley [12] studied the heat transfer from a rotating disk, assuming linear relationships between viscosity and temperature. He could express heat transfer as a series concerning both large and small Pr. Smyth and Zurita [13] numerically calculated heat transfer at a rotating cylinder's outer surface when axial flows were present. According to their results, an exponential law had good correlation with the numerical data, indicating an exponential value of 0.8. Pekdemir and Davies experimentally addressed mass transfer from a stationary circular cylinder in air submerged slot jets [14]. They reported the correlations of mean and stagnation point Sherwood numbers (Sh) using the experimental data. Laminar–turbulent transition in the boundary layer on a rough rotating disk was experimentally investigated by Zoueshtiagh et al. [15]. Using the flow visualization and hot-film measurement, they determined the transitional Re values and related boundary-layer velocity characteristics. Their results showed slight wall roughness effects on transitional Re. Seghor-Ouali et al. performed experimental observations of convective heat transfer within a rotating cylinder having an axial airflow [16] demonstrating Nu as a function of rotational and axial Re for low and high rotational speeds. Moreover, the rate of the heat transfer was merely dependent on the rotational Re. Flow and forced convection heat transfer were numerically simulated by Moshkin and Sompong in a crossflow of incompressible fluid over two rotating circular cylinders [17]. The heat transfer rates decreased by the increased cylinder rotation speed for the inter-cylinder gaps one of >1 diameter. Also, increased Pr significantly increased the average Nu while the Pr ranged between 0.7 and 50. Fenot et al. studied heat transfer between concentric rotating cylinders in the presence or absence of axial flow [18]. They well documented the dynamics of the system for a smooth closed cylindrical gap. Besides, it becomes more likely to study local heat transfer due to the significantly consistent numerical and empirical findings. Finally, they showed that complicated impacts of natural convection on flow as well as heat transfer necessitate extensive research, although these impacts are insignificant for high rotation velocities, i.e., the case in most industrial applications. Natural convection was numerically evaluated by Mahmoodi and Mazrouei Sebdani in a square cavity, in the center of which there was a nanofluid and an adiabatic square block [19]. Accordingly, the increased volume fraction reported in NPs led to an increase in Rayleigh number (Ra) in all cases, while the average Nu decreased as a function of the NP's volume fraction. Lower Ra reduces the heat transfer rates by enhancing the adiabatic square body size, whereas higher Ra values lead to its rise. Sharma and Dhiman numerically assessed the heat transfer from a circular cylinder rotating under a steady state [20]. They reported a decline in the average Nu when the rotation rates increased for the fixed Re and Pr values in the respective Re and Pr ranges of 1–35 and 0.7–100 within the steady-state flow. Moreover, a rise in the Pr enhances the average Nu under constant rotation rates and the Re values. Their results also suggest that greater Pr values reduce the average Nu more, while the rotation rate rises. Roslan et al. theoretically examined a rotating cylinder's effects on heat transfer in a square enclosure [21], in which the free space between the cylinder and the enclosure walls was filled using nonfluids which contained a combination of water and Ag, Cu, Al_2O_3, or TiO_2. Their results presented much stronger flow circulation at higher nanoparticle concentrations, better thermal conductivities, and smaller cylinders with a higher-speed and negative rotation. The highest heat transfer was reported for higher NP concentrations, also indicating desirable conductivity values. Unsteady viscous flow on a rotating stretchable disk with deceleration was numerically explored by Tiegang Fang and Hua Tao [22, 23] for a laminar and unsteady flow regime. It was possible to reduce the 3D Navier–Stokes (NS) relations into similar ordinary differential equations. They also found two branches of similarity solutions, indicating that the lower solution branch was practically impossible because of the negative velocity in the circumferential direction. Concerning the physically possible (upper) solution branch, the disk stretching and unsteadiness significantly affect the behavior of the fluid. Their results also provided a precise solution to the unsteady NS relations with novel nonlinear phenomena and several solution branches. Harmand et al. investigated fluid flow and convective heat transfer in the case of rotating disk cavities with jet impingement. They focused on convection heat transfer in principally outward airflow in the rotor–stator

geometries in the presence and absence of jet impingement, incorporating two primary parts (empirical/theoretical methods and geometries/results). Dipankar Chatterjee et al. performed numerical investigation of mixed convection transport in a lid-driven cavity, at the center of which there was a nanofluid and a rotating circular [24]. Their simulations were carried out for the Richardson number (Ri), dimensionless rotational speed, and nanoparticle concentrations ranging 1–10, 0–5, and 0–0.2, respectively. The average Nu on the heated topmost enclosure lid increased by Ri enhancement. This value initially decreased to the lowest but increased by the cylinder rotation. Lower dimensionless rotational speeds led to a maximum heat transfer. Bouakkaz et al. numerically calculated the rotation rate effects on the laminar flow and heat transfer passing a circular cylinder [25]. The average Nu decreases as the rotation rate increases and faces an increase as the Re goes up. The second type of instability appeared at faster rotations shedding a series of counterclockwise vortices in the upper shear layer. Capone et al. experimentally investigated the flow phenomenology around a circular cylinder at subcritical and critical Re [26]. According to them, the approach of Re to the critical state leads to a growingly weaker spectrum peak featured by the separation line oscillations in comparison with the near-wake velocity spectrum. There was a significant reduction in the separation line oscillations under the critical regime, leading to correlations with the local vorticity. Kareem and Gao numerically addressed the mixed convection heat transfer of turbulent flow in a 3D lid-driven cavity with a rotating cylinder. An overall decrease showed modifications in the vortex shedding [27]. They also carried out the performance evaluation for two turbulence techniques, LES and URANS, demonstrating the significant impacts of increased the rotating cylinder's speed or Re on the flow patterns and thermal fields. They also presented conclusive proof on the ability of LES in predicting the structural specifications of the secondary eddies with considerable impacts on the heat transfer behaviors in an enclosure. Fluid flow and heat transfer for the case of a rotating and vertically moving disk were evaluated byTurkyilmazoglu [28]. As the disk moves upwards and downwards, some impacts similar to those of the injection/suction are exerted through the walls, although considerable differences can be observed. Besides, there a jet-like radial velocity was reported for the viscous pumping by the rapid upward movement of the disk. Even though the disk downward movements suppressed the velocity field, increased thickness of boundary layer is anticipated, unlike the conventional wall suction. Furthermore, the temperature field showed high dependence on the wall temperature, sustained at a time-varying function. Barati et al. numerically assessed the rotational direction impacts in the case of a circular cylinder for mixed convection at subcritical Re [29]. It was demonstrated that counting the buoyancy force excitation causes vortex shedding. The rotation of the cylinder also increased the absolute lift coefficients and decreased the drag coefficients compared to the stationary cylinder. The rotating cylinder's Nu (in both rotation directions) was decreased compared to a stationary cylinder which consequently decreased heat transfer. Forced convection heat transfer was numerically evaluated for a rotating elliptic cylinder in the laminar flow state by Kumar and Kumar Sahu [30]. At a constant Pr value, the average Nu underwent a linear increase with increased Re. Besides, at a constant Re values, the Nu values increase under an increasing Pr. Moreover, the thinning of the thermal boundary layer takes place on the cylinder's rear side by enhancing the Pr number at a constant Re number, subsequently increasing the local Nu and temperature gradient. Chen and Zhang numerically examined the rotation number impacts on flow and heat transfer in contra-rotating disk cavities with the superposed flow [31]. They focused on the rotation number impacts on the structure of the flow, performance of cooling, effects of sealing, and characteristics of surface tangential friction within the cavity. They concluded that at the rotation numbers < 1, the fluids in the core region between two disks rotate with the upstream disk similar to a rigid body, and the rotating core's tangential velocity reduces with enhancing the disk cavity radius, showing difference from the Batchelor-type flow. Considering the rotation numbers > 1, the fluids on the upstream side of the disk rotate similar to the Batchelor-type flow, whereas the sandwich rotation will disappear in the fluid on the downstream side of the disk. Mixed convection heat transfer from a circular cylinder submerged in a wake was numerically investigated by Farhan Zafar and Mahbub Alam [32]. The impacts of Ri ($=0$–2.0) were addressed on the flow and heat transfer topologies of a circular cylinder submerged in the wake of another cylinder at $\mathrm{Re} = 100$. By enhancing Ri, downwash and upwash flows were created prior and following the heated cylinder, respectively, increasing the heat transfer from the cylinder. Moreover, the Ri impact was entirely passed on aerodynamic parameters, consisting of fluid forces, Strouhal numbers, Nu, and Reynolds stresses. Convective heat transfer and flow phenomena from a rotating sphere in porous media were analytically studied by Safarzadeh and Rahimi [33]. The analytical solution of the equation was according to power series, and the porosity coefficient was presumed to range from 0 to 1. The azimuthal angle direction changes were overlooked, while the body force and pressure gradient were considered zero. They showed an increment in velocity and vortex diffusion in the boundary layer by raising the Re; hence, the boundary layer thickness grows. The increased Re also enhances the velocity gradient within the boundary layer, leading to an increase in temperature gradients. Chen et al. performed numerical investigations of mixed convection between a rotating sphere and a concentric cubical

enclosure [34]. They assessed the rotational direction, Ra, and rotational Re impacts on heat transfer. The inner sphere rotationality increased the system's global heat transfer rate, while the rotating motion stimulated heat transfer in the rotational axis radial direction and surpassed the thermal expansion in the axial direction. Pantokratoras numerically studied forced convection heat transfer from a heated rotating sphere in laminar flow [35]. He solved the heat problem and significant differences among his findings and of the study conducted by Feng [36], reporting a value of 38% for the isothermal case. Regarding the proper agreement between his fluid results and previous papers, his findings on the average Nusselt were considered new reference values. Mohammed Jabbar et al. [37] studied thermal analysis of nanofluid saturated in inclined porous cavity cooled by rotating active cylinder subjected to convective condition. They filled the porous cavity with copper–water nanofluid. All walls of the cavity are thermally isolated except bottom wall that moving to the right and has high temperature. They reported the effects of Richardson number, Darcy number, inclination angle, conductivity ratio, rotational speed, and nanofluid volume fraction. They were able to increase the average Nusselt number by 223% by increasing the rotation speed. Also, their result shown that Richardson number has bad effect on average Nusselt number.

Somayeh Davoodabadi and Hakan F. Oztop [38] investigated the effect of changing in the width of the cavity, the radius of the rotational and vibrational cylinder, and the effect of the rotational speed on natural convection in a rectangular tall cavity. They assumed the vibration of the cylinder in the Y-direction and in a sinusoidal form. Their result shown that as the angular velocity, the vibration amplitude and frequency increases, the heat transfer rate increases.

According to the literature review, most of the papers have addressed two-dimensional problems. Three-dimensional mix convection from a rotating vertical cylinder has not been investigated in a resting fluid without the effect of walls. The effect of LES and URANS turbulence models in the simulations of these problems was also neglected. Thus, this paper is aimed to fill this gap.

Numerical model

Geometry

Figure 1 depicts the geometrical configuration and main parameters of a three-dimensional rotating vertical cylinder concentric with an outer cylinder (chamber). Figure 1a and b represents the inner and outer vertical cylinders, respectively. S_i and S_o show the half-height of cylinders, w denotes the rotational speed, while r and z represent cylindrical coordinate systems. The symbol I denotes the regions above and below the inner cylinder whereas the annular region is shown by Π. The domain walls have been considered stationary and thermally cold with a constant temperature, while the vertical cylinder is treated as a hot rotating wall at a constant temperature.

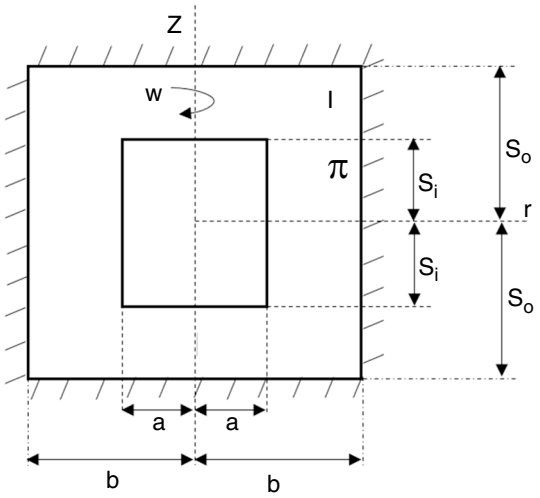

Fig. 1 Geometry and main geometrical parameters

Governing equation

The main continuity, momentum, and energy equations used for 3D turbulence flow and heat transfer within unsteady-state flow, viscous incompressible fluid, laminar and turbulent flow, no-slip, and isothermal boundary conditions are imposed on both boundaries, and changes in the thermodynamic properties of the fluid are assumed to be insignificant and constant are as follows [27, 39–41]:

Continuity Eq:

$$\frac{1}{\rho}\frac{\partial \rho}{\partial t}+\frac{1}{r}\frac{\partial}{\partial r}\left(rv_{\mathrm{r}}\right)+\frac{1}{r}\frac{\partial v_{\theta}}{\partial \theta}+\frac{\partial v_{\mathrm{z}}}{\partial z}=0 \tag{1}$$

Momentum Eq:

R–direction:

$$\frac{\partial v_{\mathrm{r}}}{\partial t}+(v.\nabla)v_{\mathrm{r}}-\frac{1}{r}v_{\theta}^{2}=-\frac{1}{\rho}\frac{\partial p}{\partial r}+g_{\mathrm{r}}+\vartheta\left(\nabla^{2}v_{\mathrm{r}}-\frac{v_{\mathrm{r}}^{2}}{r^{2}}-\frac{2}{r^{2}}\frac{\partial v_{\theta}}{\partial \theta}\right) \tag{2}$$

θ-direction:

$$\frac{\partial v_{\theta}}{\partial t}+(v.\nabla)v_{\theta}-\frac{1}{r}v_{\mathrm{r}}v_{\theta}=-\frac{1}{\rho r}\frac{\partial p}{\partial \theta}+g_{\theta}+\vartheta\left(\nabla^{2}v_{\theta}-\frac{v_{\theta}}{r^{2}}+\frac{2}{r^{2}}\frac{\partial v_{\mathrm{r}}}{\partial \theta}\right) \tag{3}$$

Table 1 optimal mesh numbers with comparison of average Nusselt number at the surface of vertical rotational cylinder

Mesh	8,54,210	11,85,632	14,73,920	16,45,125
Average Nusselt number	434.175	450.856	474.9877	488.324
Error/%	11.1	7.7	2.7	–

z–direction:

$$\frac{\partial v_z}{\partial t} + (v.\nabla)v_z = -\frac{1}{\rho}\frac{\partial p}{\partial z} + g_z + \vartheta\nabla^2 v_z - g\beta\left(T - T_c\right) \tag{4}$$

Energy Eq:

$$\rho C_p\left[\frac{\partial T}{\partial t} + (v.\nabla)T\right] = k\nabla^2 T \tag{5}$$

where ρ, g, and v represent the density, gravitational acceleration, and kinematic viscosity of fluid, respectively. The quantities u_r, u_z, u_θ show the components of velocity in the r, z, and θ directions, while β indicates the thermal expansion coefficient. k and C_p represent the thermal conductivity and constant pressure specific heat coefficient of fluid, respectively. In cylindrical coordinates, the divergence $(V.\nabla)$ and ∇^2 operators are defined as follows:

$$V.\nabla = v_r\frac{\partial}{\partial r} + \frac{1}{r}v_\theta\frac{\partial}{\partial\theta} + v_z\frac{\partial}{\partial z} \tag{6}$$

$$\nabla^2 = \frac{1}{r}\frac{\partial}{\partial r}\left(r\frac{\partial}{\partial r}\right) + \frac{1}{r^2}\frac{\partial^2}{\partial\theta^2} + \frac{\partial^2}{\partial z^2}$$

The turbulence equations in the URANS and LES models are as follows:

URANS model

To simulate the URANS model, the standard k- ε model has been used, whose equations are given below: [17, 42]

$$\begin{aligned}&\frac{\partial}{\partial t}(\rho k) + \frac{\partial}{\partial x_i}\left(\rho k u_i\right)\\ &= \frac{\partial}{\partial x_j}\left[\left(\mu + \frac{\mu_t}{\sigma_k}\right)\frac{\partial k}{\partial x_j}\right]\\ &+ P_k + P_b - \rho\varepsilon + S_k\end{aligned} \tag{7}$$

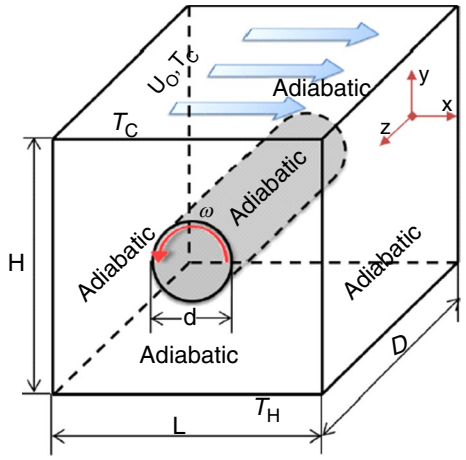

Fig. 2 Schematic geometry of validation case [27]

$$\begin{aligned}&\frac{\partial}{\partial t}(\rho\varepsilon) + \frac{\partial}{\partial x_i}\left(\rho\varepsilon u_i\right)\\ &= \frac{\partial}{\partial x_j}\left[\left(\mu + \frac{\mu_t}{\sigma_k}\right)\frac{\partial k}{\partial x_j}\right]\\ &+ C_{1\varepsilon}\frac{\in}{k}\left(P_k + C_{3\varepsilon}P_b\right) - C_{2\varepsilon}\rho\frac{\in^2}{k} + S_\varepsilon\end{aligned} \tag{8}$$

where S_k and S_ε are user-defined source terms and $C_{1\varepsilon}$, $C_{2\varepsilon}$ and $C_{3\varepsilon}$ are model constants. However, the other parameters define below:

$$\text{Turbulent viscosity: } \mu_t = \rho C_\mu\frac{k^2}{\varepsilon} \tag{9}$$

$$\text{Production of } k: P_k = -\rho\overline{u_i' u_j'}\frac{\partial u_i}{\partial x_i} \tag{10}$$

$$\text{Effect of buoyancy}: P_b = \beta g_i\frac{\mu_t}{Pr_t}\frac{\partial T}{\partial x_i} \tag{11}$$

LES model

For setting up parameters for the LES model, we utilized the sub-grid scale model of wall-adapting local eddy viscosity, according to literature. [43, 44]

$$\mu_t = \rho L_s^2\frac{\left(S_{ij}^d S_{ij}^d\right)^{\frac{3}{2}}}{\left(\overline{S}_{ij}\overline{S}_{ij}\right)^{\frac{5}{2}} + \left(S_{ij}^d S_{ij}^d\right)^{\frac{5}{2}}} \tag{12}$$

where L_s and $S_{ij}^d S_{ij}^d$ have the following definitions:

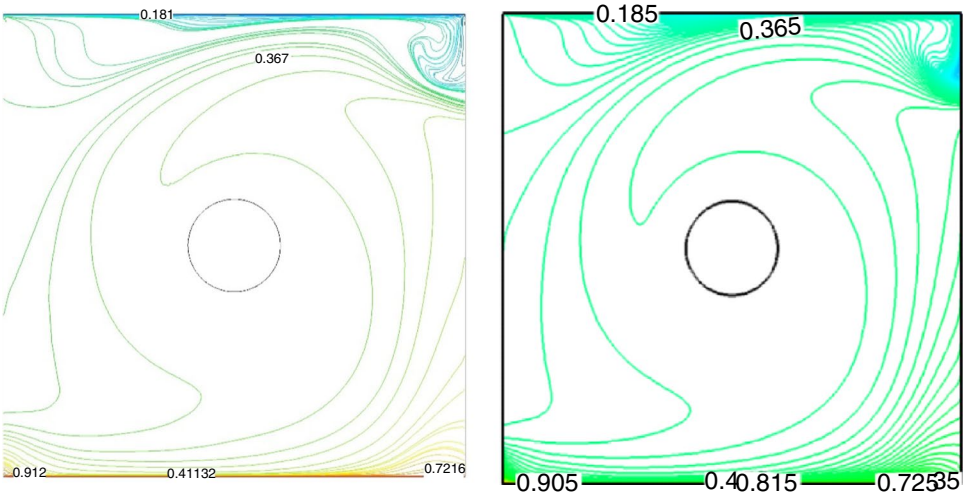

Fig. 3 Compression between: left, present work of isotherm, and right: Ali Khaleel Kareem and Shian Gao [27]

Table2 Compression between present work of dimensionless velocity profiles along the vertical line at $x=0.25$ with Ali Khaleel Kareem and Shian Gao [27]

Different position along vertical line at $x=0.25$	Local Nusselt number		
	Present study	Chuan-Chieh Liao, Chao-An Lin [29]	Error/%
0	0.0068	0.007	2.86
0.05	0.0089	0.009	1.11
0.1	0.0098	0.01	2
0.15	0.01048	0.0105	1.9
0.2	0.01071	0.0108	0.8
0.25	0.01032	0.0107	3.6
0.3	0.0095	0.0101	5.9
0.35	0.0089	0.0092	3.3
0.4	0.00668	0.007	4.6
0.45	0.00369	0.0038	2.9
0.5	-0.000791	-0.0008	1.1
0.55	-0.00507	-0.005	1.4
0.6	-0.009	-0.0088	2.3
0.65	-0.0115	-0.0112	2.7
0.7	-0.0128	-0.0125	2.4
0.75	-0.0138	-0.0133	3.8
0.8	-0.0137	-0.0134	2.2
0.85	-0.0129	-0.0126	2.4
0.9	-0.0091	-0.0089	2.2
0.95	-0.00174	-0.0017	2.3
1	0.0156	0.015	4

Table 3 compression between average Nusselt number at different aspect ratio

b/*a*	Average Nusselt number	Error/% with increases *b*/*a* to			
		3	4	5	6
3	433.4147	–	8.8	11.3	12.3
4	474.9877	–	–	1.6	2.5
5	482.504	–	–	–	0.8
6	486.7981	–	–	–	–

Table 4 compression between laminar and turbulent flow at the different Reynolds number

Re	Average Nusselt number		Error/%
	Laminar simulation	Turbulent simulation	
200	481.32	–	–
500	503.58	474.99	5
700	553.34	495.35	10.5
1000	472.71	662.03	28.6

$$L_s = \min\left(kd, C_w V^{\frac{1}{3}}\right) \tag{13}$$

where

$$C_w = 0.325$$

$$S_{ij}^{d} = \frac{1}{2}\left(\bar{g}_{ij}^{2} + \bar{g}_{ji}^{2}\right) - \frac{1}{3}\delta_{ij}\bar{g}_{kk}^{2} \tag{14}$$

where

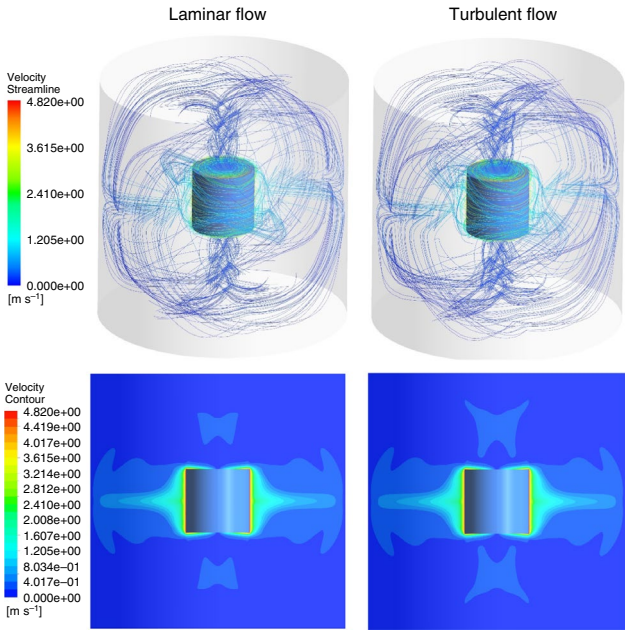

Fig. 4 Comparation between laminar and turbulent flow at the Re = 1000

$$\overline{g}_{ij} = \frac{\partial \overline{u}_i}{\partial x_i} \tag{15}$$

$$\overline{S}_{ij} = \frac{1}{2}\left(\frac{\partial \overline{u}_i}{\partial x_j} + \frac{\partial \overline{u}_j}{\partial x_i}\right) \tag{16}$$

Boundary condition

These conditions have the following definition for the governing equations:

Domain walls:

$$T = T_C = 300\text{K},\ u = 0,\ v = 0,\ w = 0$$

Cylinder:

$$w = \frac{4\text{Re}.\vartheta}{a^2},\ a = 0.25\ b,\ T = T_H = 360\text{K}$$

where a and b represent the inner and outer vertical cylinder radius. T_H and T_c show the inner and outer vertical cylinder temperatures, respectively.

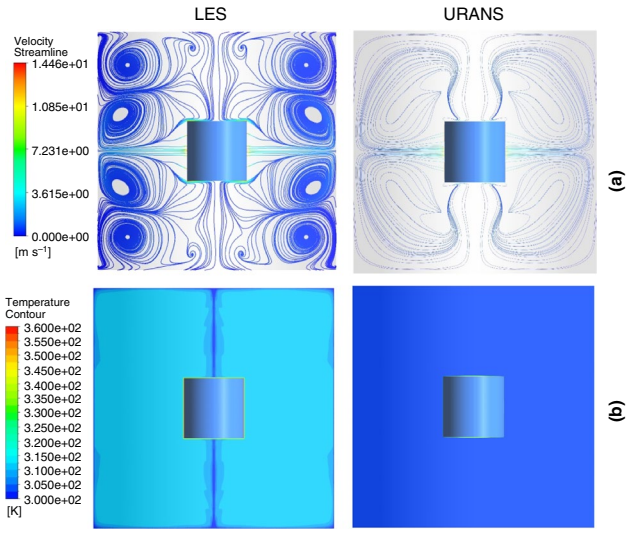

Fig. 5 Comparison between LES and URANS turbulency models at XY plane locate $Z = 0$: **a**. streamline, **b**. isotherm contour

Numerical procedure

The computational fluid dynamic (CFD) was utilized for numerical assessment of fluid flow and heat transfer. The governing equations were discretized based on the pressure–velocity coupling equation with the method of finite volume and SIMPLEC algorithms. The commercial code ANSYS©FLUENT (Release 18.1) [45] was employed to solve the equations. A QUICK and implicit second-order scheme was applied for unique discrete parameters for solving both the URANS and the LES equations at Re = 3000. The simulation is terminated when reaching the absolute convergence criterion of 10–5 for all the parameters at every time step.

Results and discussion

The effect of rotation of the vertical cylinder in a resting fluid on heat convection and turbulent flow patterns is addressed in this section. The simulations include five Reynolds numbers, Re = 200, 500, 1000, 1500, 2000, and 3000. The fluid is an engine oil whose all parameters are taken constant and do not change with temperature. Only the density follows the Boussinesq approximation.

Independence of mesh

Mesh independence is one of the crucial parameters in the simulations with a significant impact on the accuracy and convergence time. The ICEM 18.1 software was utilized for the structure and non-structured cells. In the area near the rotating cylinder, the mesh is refined. The dimensions of

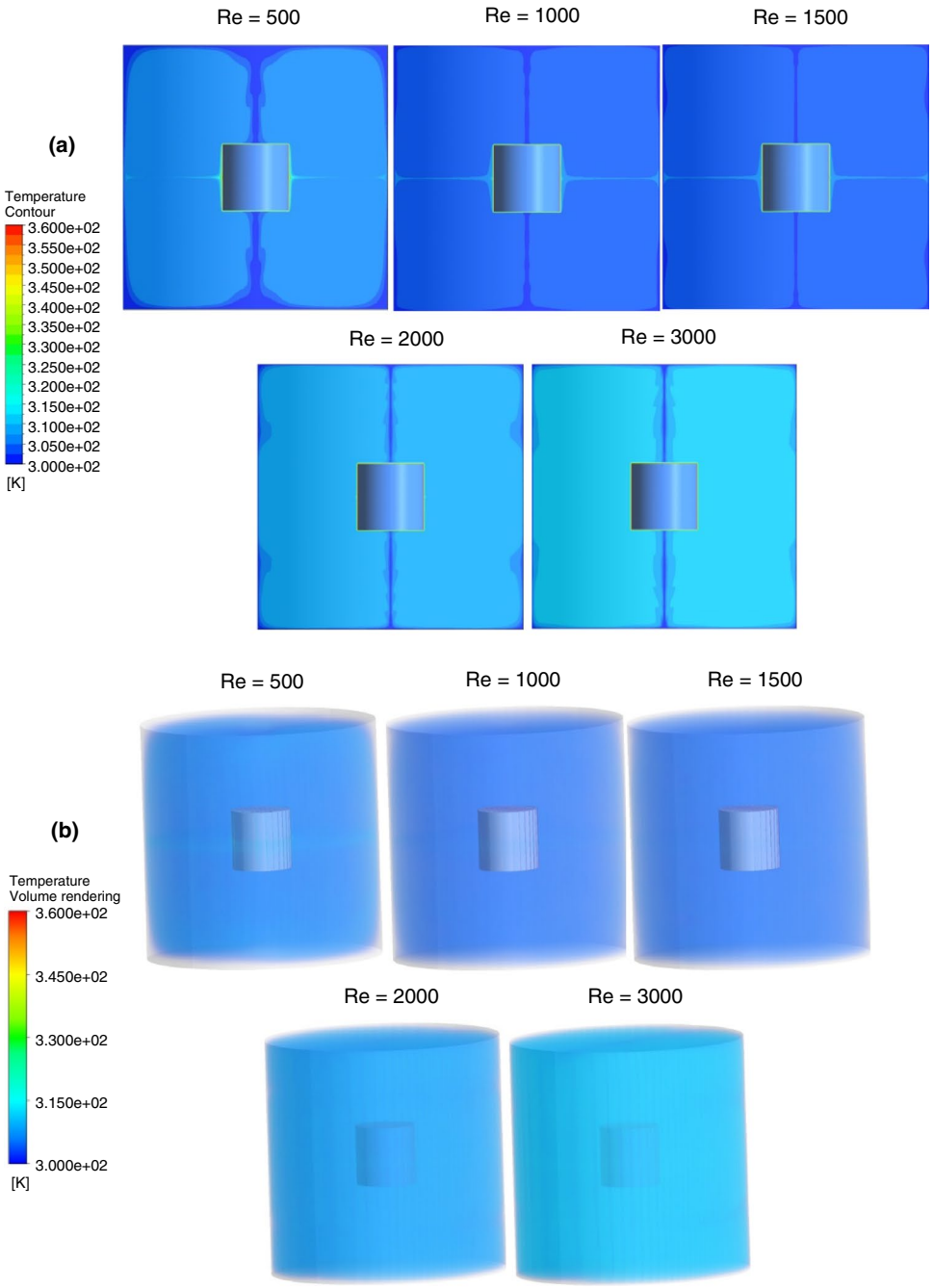

Fig. 6 Effect of Re number on the flow parameters: **a** 2D isotherm in *XY* plane locate at middle of *Z* plane, **b** 3D temperature contour, **c** 2D velocity contour in *XY* plane *XY* plane locate at middle of *Z* plane

the cells increase slowly as it moves away from the rotating vertical cylinder. Four grid numbers (8,54,210, 11,85,632, 14,73,920, and 16,45,125) were tested to calculate the average Nusselt number on a vertical rotational cylinder in $\lambda = 4$ and the $\mathrm{Re} = 500$ to find the optimal mesh numbers. Comparing accuracy and convergence time, the grid number of 14,73,920 was selected (Table 1).

Validations

Simplification and comparison of the developed model were carried out with the results obtained by Kareem and Gao [27] to validate heat convection and flow pattern under turbulent conditions. Comparisons were made based on

Fig. 6 (continued)

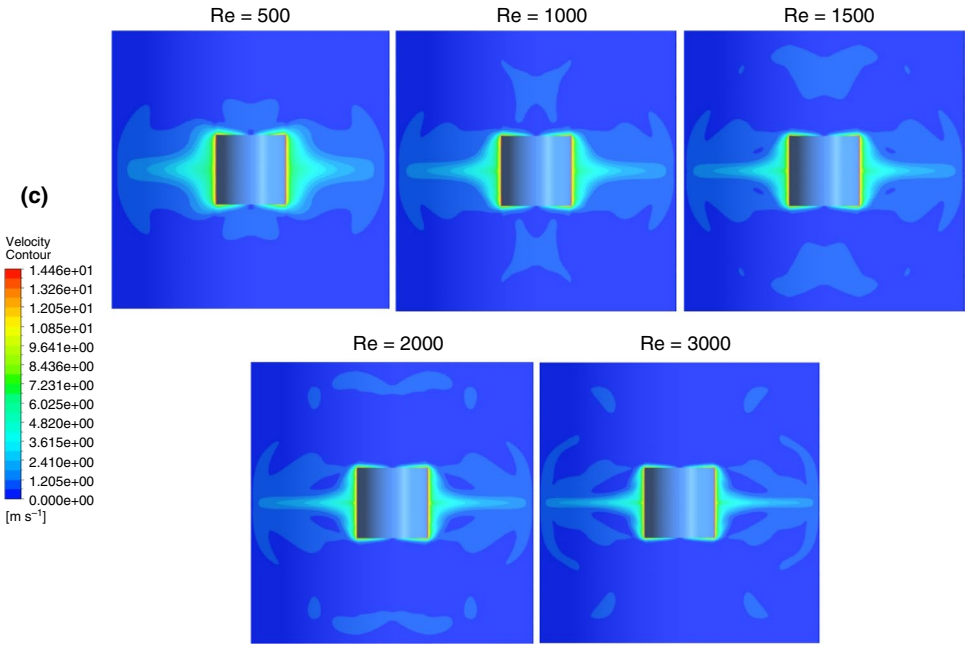

dimensionless parameters of $Gr = 10^4$, $Re = 30{,}000$, and $(\Omega) = 10$. The validated case is shown in Fig. 2.

The LES model was employed for turbulence, and the obtained results were compared with previous reports [27] concerning isotherms and dimensionless velocity profiles across the vertical line for $x = 0.25$ which exhibited acceptable consistency, according to Fig. 3 and Table 2.

Independence of domain

In this section, the effect of the walls domain on simulation is investigated at $Re = 500$. The comparison is made for aspect ratios of $\lambda = 3$, 4, 5, and 6. A. As shown in Table 1, a rise in the aspect ratio above 4, led to less than a 3% difference in the average Nu than the case of $\lambda = 4$. Therefore, the aspect ratio of 4 was considered to reduce the convergence cost and time (Table 3).

Changing flow from laminar to turbulency

In this section, the flow regime changes from laminar to turbulent by altering the Reynolds number. For this purpose, simulations were performed from the $Re = 200$, and the streamline and contours of velocity were investigated. Based on the results, secondary vortices are forming, and the flow is turbulent at $Re = 1000$. Comparisons of the average Nu revealed a very high error upon the wrong choice of flow regime at $Re = 1000$ which can be due to the rise in the flow movement upon flow variation from laminar to turbulent (Table 4).

According to Fig. 4, the fluid movement increases at the uppermost and bottom of the vertical rotating cylinder for turbulent flow which enhanced the average Nusselt.

Comparison between result from LES and URANS turbulency model

In this section, we want to compare the results obtained from the simulation of two methods, The LES model against an URANS-based RNG k-ε model, so that we can obtain and evaluate the results more accurately by choosing the appropriate model. For $Re = 3000$, the rotating of a vertical cylinder is known to be turbulent flow. Therefore, the simulation is complete for both methods at this Reynolds number. The LES model can improve the prediction capability by the better illustration of secondary flow and

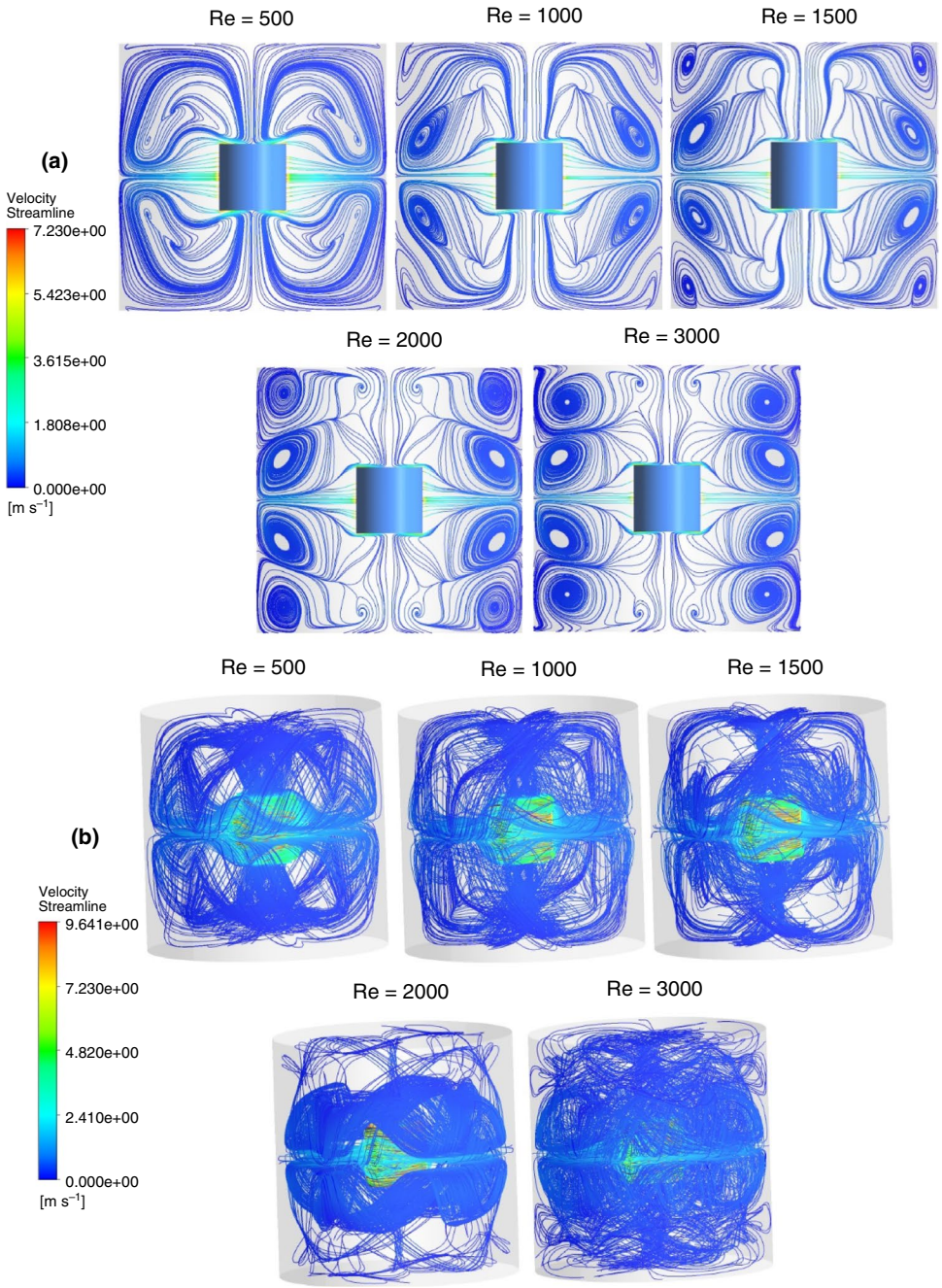

Fig. 7 Flow comparison at different Re number: **a** 2D streamline in *XY* plane locate at middle of *Z* plane **b** 3D streamline

forming swirling eddy in a domain. Thus, the heat transfer diffuser also increases as displayed in Fig. 5.

A comparison between the behavior of the two models (Fig. 6) shows that the URANS model cannot properly simulate the physics of the problem including the secondary flow and heat transfer. However, it can be predicted that the vorticities grow with increasing Reynolds number or increasing rotational speed, so the LES method was used in these studies due to its ability to predict vorticities.

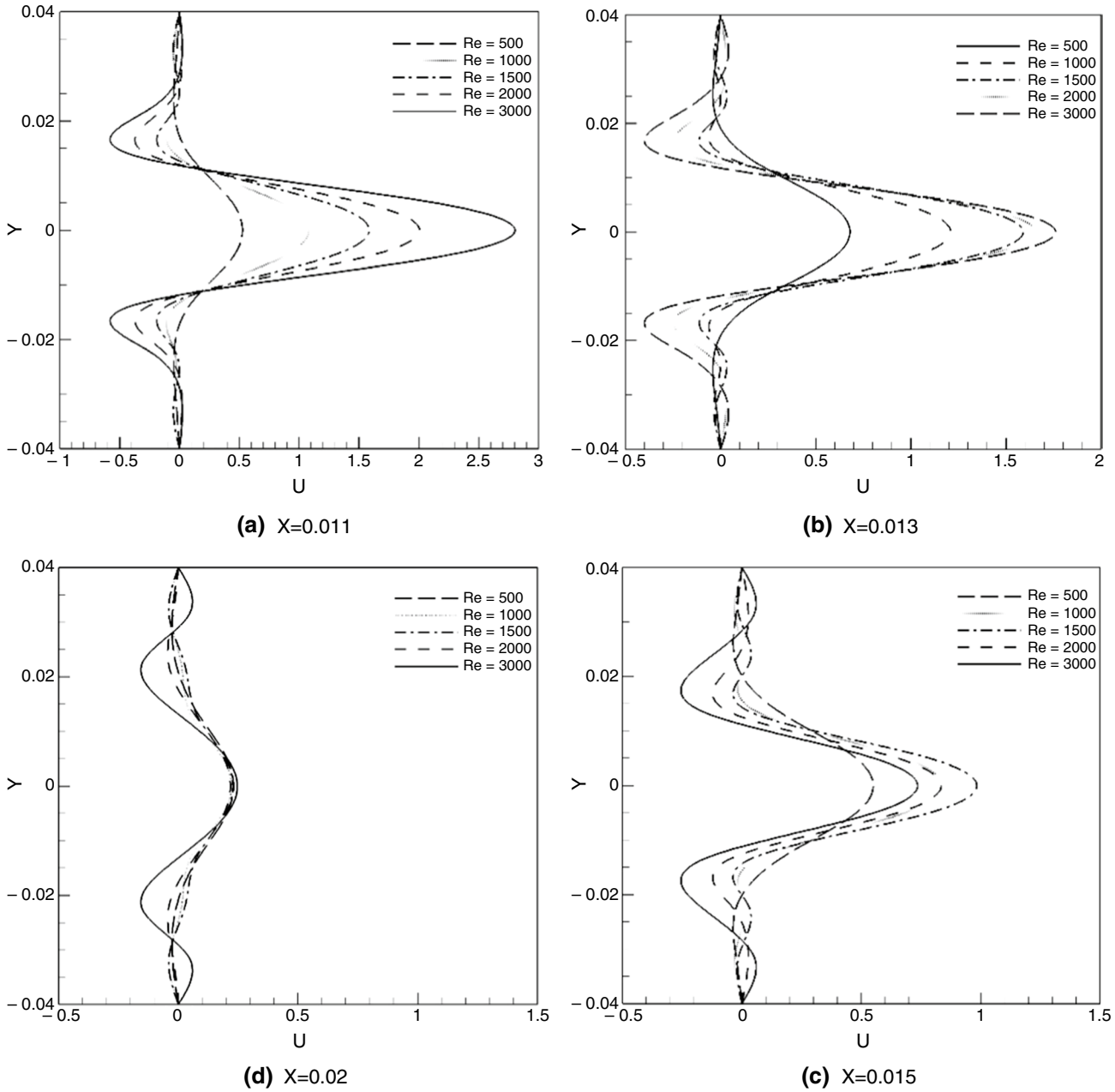

Fig. 8 Velocity distribution along the different vertical line for different Reynolds numbers

LES model

Flow and thermal fields

Figure 6 shows 2D and 3D isotherms and streamline for different controlling parameters concerning the Re ranges of 500–3000. The results were achieved considering the effect of shear force (from the rotational vertical cylinder) and the buoyancy flow (from the temperature differences of the rotating vertical cylinder and domain walls). Noteworthy, the impact of shear force is dominant as the Reynolds number increases.

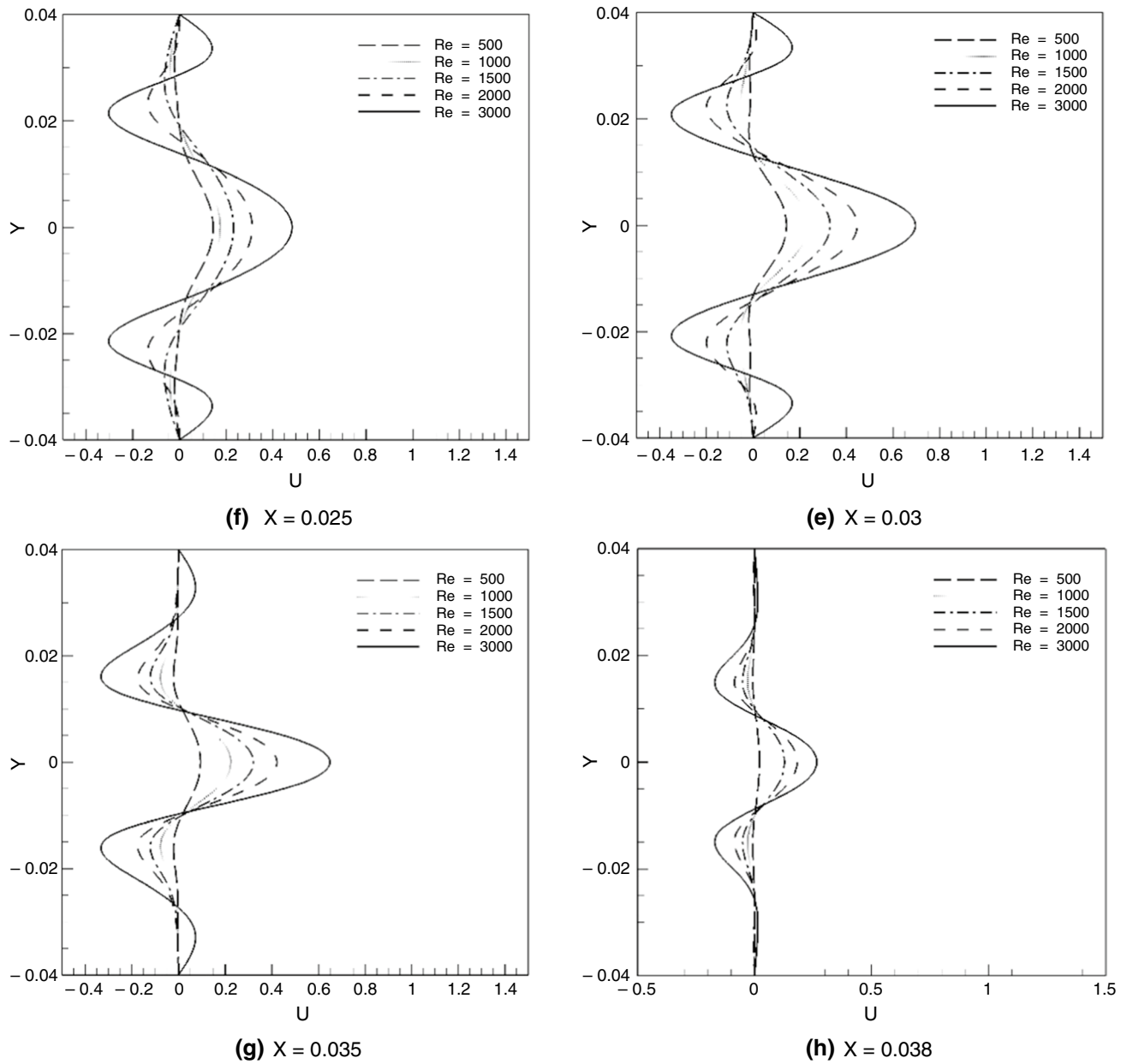

Fig. 8 (continued)

As seen, by increasing the Reynolds number (rotation speed), the flow from the vertical cylinder's uppermost and bottom is launched in the axial direction approaching the cylinder's center while a jet-like flow is formed from the center in the radial direction. The Re influence on this phenomenon is evident in the velocity contour represented in Fig. 6c. This phenomenon will guide the flow to move in the domain and increase the heat transfer, and thus, the movement will enhance in the domains as Re (rotation speed) increases. Besides, the heat transfer and the temperature also show a rising trend; their isotherm contours are shown in Fig. 6a and b. The symmetric results in the r-direction (Fig. 8) suggest the minimal buoyancy impact on heat transfer while the predominant phenomenon of forced convection is due to the vertical cylinder's rotation.

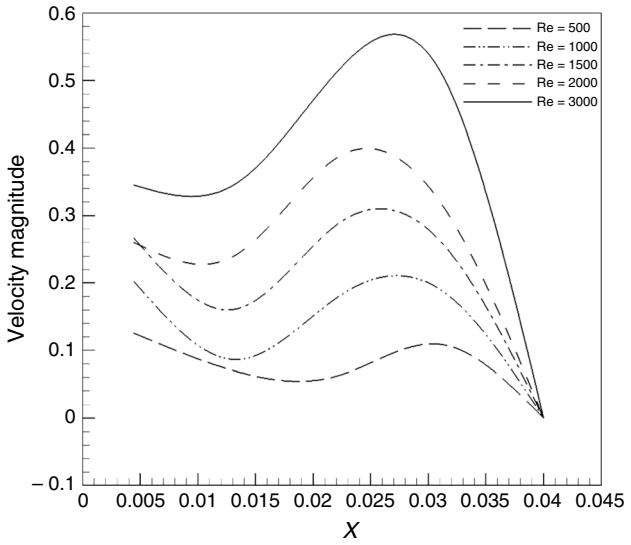

Fig. 9 Velocity distribution along the $y = 0.015$ for different Reynolds number

Figure 7 indicates the structure of flow patterns on the *XY* plane at the center of the *Z*-axis and 3D streamline for different Reynolds numbers. At Re = 500, the rotational flows are generated at the cylinder's upper and lower areas. An increase in the rotation speeds up to Re = 1000 leads to the formation of counterclockwise secondary eddies. Further increase in the rotation speed to Re = 1500 enhances the intensity of these eddies, moving more flows toward these eddies. This movement results in other secondary eddies in the corner of the domain. Further increment of the rotational speed beyond Re = 1500 enhances the secondary eddies in the corners. At Re = 3000, the size and intensity of the secondary eddies are almost equal to each other. As shown in Fig. 7b, the increase in motion created by these eddies increments the heat transfer and the relative temperature throughout the domain.

Velocity distribution

The dimensionless velocity on vertical lines is plotted in Fig. 8 at different radial positions relative to the axis of the rotating vertical cylinder for different Re values (500–3000). As explained above, since the flow in the direction of the axis is approaching the center of the vertical cylinder and throws it out due to rotation, the maximum velocity in different positions is related to the center of the lines. Also, with increasing the Re number, as expected, the highest speed in different places is observed at Re = 3000. This phenomenon is near the vertical cylinder ($X = 0.011$ to $X = 0.015$) due to the suction of flow to the center of the

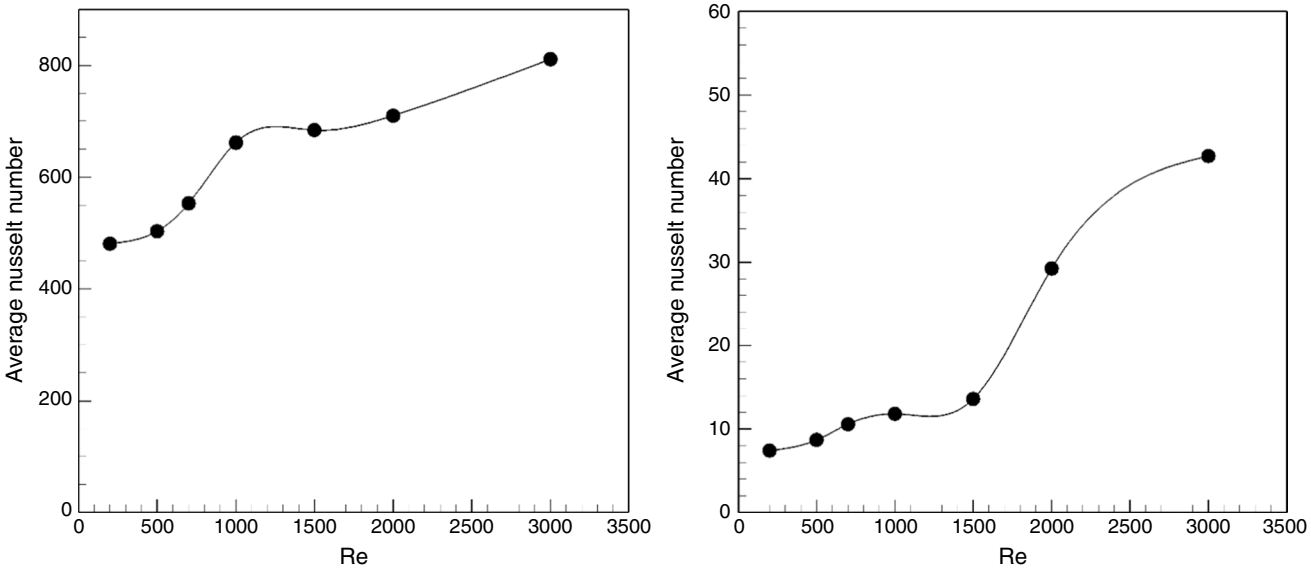

Fig. 10 The relationship between average Nusselt number (Nu_{ave}) and Reynolds number (Re): left rotational vertical cylinder, right domain's wall

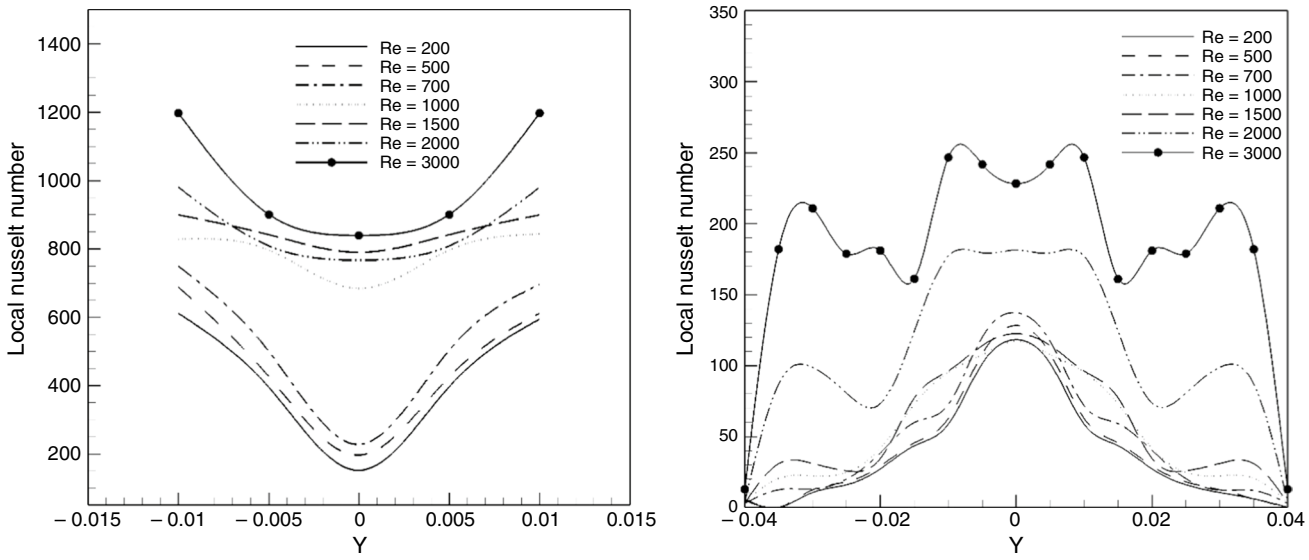

Fig. 11 The relationship between local Nusselt number (Nu_{Local}) and Reynolds number (Re): left rotational vertical cylinder, right domain's wall

rotation. In lines farther from the center, this phenomenon can be due to the proximity of secondary eddies, as seen in Re < 2000 (9d-9 h). At Re = 3000, due to the magnitude of these eddies, the return velocity is approximately equal to the flow velocity at the center. The effect of secondary eddies in the corners of the domain can be observed from $X = 0.02$ in Re = 3000.

Figure 9 shows the trend of velocity along the line $Z = 0.015$ in the positive direction of the X-axis. Noteworthy, the velocity increase in the area of secondary vortices is in the range of 0.02–0.03.

Heat transfer

Figure 10 displays the variations of the mean Nu for different Reynolds numbers (200–3000). A rise in the Reynolds number enhances the average Nu on the rotating vertical cylinder and the boundary walls. As the Re values rise, the flow movement grows more, which enhances the heat transfer, implying the necessity to increase the average Nu as Re increases. The important point in the average Nu changes is the significant increase in its value from Re = 2000 to Re = 3000 (~ 14.3% for the rotational vertical cylinder). This trend can be attributed to the increase in the intensity of the secondary eddies in the corners of the domain and those near the center line. An increment in Reynolds number from 200 to 3000 increases the average Nu by 68% for rotational vertical cylinder and 475% for domain's wall.

Figure 11 depicts the local Ne across the longitudinal axis of the vertical rotating cylinder and the walls of the domain considering various Reynolds numbers. The fluid is thrown out more by enhancing the Re, resulting in the lower fluid volume in the center of the rotating vertical cylinder compared to the vertical walls, and thus, the local Nu in this area will be less than the distant points from the center. This difference becomes more as Re increases. On the boundary walls, this trend is different such that the greatest heat transfer rate with the boundary walls can be observed at the center. In areas far from the center and at low Re, the local Nu rate decreases, while this decrease is very small at Rey = 3000 near the center. At Re = 3000, the creation of secondary eddies in the corners of the domain again increments the local Nu in these areas.

Conclusions

The turbulent flow and three-dimensional heat transfer of a rotating vertical cylinder have been simulated within a static fluid using the finite volume method. The Re (rotational speed) effects on the physics of the problem were explored. LES and URANS methods have been also evaluated to simulate turbulence. The results show exciting behaviors of turbulent flow and heat field in the problem, which can be summarized as follows:

(1) According to the average Nu changes against the Re, the flow regime shifts from laminar to turbulent at Re = 1000.
(2) At high Reynolds numbers, the URANS method cannot simulate secondary eddies while LES displays more

flow and secondary eddies details, despite its longer solution time and computational cost compared to the RARNS method. Therefore, the LES method was used in all simulations of this research.

(3) The velocity distribution and flow structure strongly depend on the Reynolds number. A rise in the Reynolds number guides the flow along the axis of the vertical cylinder toward the center and throws it out of the center to the radial direction. Enhancement of the Reynolds number forms secondary eddies in the solution domain. By raising the rotational speed to the Re = 2000, the intensity of these eddies rises. Beyond Re = 2000, other secondary eddies are formed in the corners of the domain, such that at Re = 3000, the intensity and magnitude of these secondary eddies are approximately equal to the central secondary eddies.

(4) Re enhancement increases the heat transfer rate and the average Nu. A 71% increment can be detected in the average Nu as Re increases from 500 to 3000 due to the increase in the motion of the fluid.

(5) The effect of the buoyancy force is almost eliminated at Re > 500, and the domain is affected by the rotation of the vertical rotating cylinder.

References

1. Weaver DS, Miskovic S. 'A study of RANS turbulence models in fully turbulent jets: a perspective for CFD-DEM simulations.' MDPI J Fluids. 2021;6:271. https://doi.org/10.3390/fluids6080271.
2. Iaccarino G, Marongiu C, Catalano P, Amato M. RANS simulation of the separated flow over a bump with active control. Capua CE Italy: CIRA Inc; 2003.
3. Ramesh V, Vengadesan S, Narasimhan JL. 3D unsteady RANS simulation of turbulent flow over bluff body by non-linear model. Int J Numer Methods Heat Fluid Flow. 2006;16(6):660–73. https://doi.org/10.1108/09615530610679048.
4. Moeng C-H. A large eddy simulation model for the study of planetary boundary layer turbulence. Hornal Atmos Sci. 1984. https://doi.org/10.1175/1520-0469(1984)041%3c2052:ALESMF%3e2.0.CO;2.
5. Hajipour A, Lavasani AM, Yazdi ME, Mosavi A, Shamshirband S, Chau K-W. Simulation of turbulent flow around a generic high-speed train using hybrid models of RANS numerical method with machine learning. arXivLabs Journal, 2019. https://doi.org/10.48550/arXiv.2001.01569.
6. Som S, Senecal PK, Pomraning E. Comparison of RANS and LES turbulence models against constant volume diesel experiments. In: 24th Annual conference on liquid atomization and spray systems, San Antonio, TX; 2012. http://www.ilass.org/2/conferencepapers/65.pdf.
7. Ishihara T, Qian GW, Qi YH. Numerical study of turbulent flow fields in urban areas using modified k-ε model and large eddy simulation. J Wind Eng Ind Aerodyn. 2020;206:10433. https://doi.org/10.1016/j.jweia.2020.104333.
8. Vatsa VN, Lockard DP. Assessment of hybrid RANS/LES turbulence models for aeroacoustics applications. In: 16th AIAA/CEAS aeroacoustics conference, Stockholm, Sweden, 2010. https://doi.org/10.2514/6.2010-4001.
9. Guilmineau E, Deng GB, Queutey P, Visonneau M, Wackers J. Assessment of turbulence models for flow around three-dimensional geometries. Numer Fluid Mech Multidiscip Des. 2018. https://doi.org/10.1007/978-3-319-70031-1_21.
10. Abbassi A, Zgolli R. A large eddy simulation model for simulation of turbulent flow in a converging-diverging nozzle. In: 24th Conference of mechanics, Brest, 2019. https://cfm2019.sciencesconf.org/254372/document.
11. Frazer RA. On the motion of circular cylinders in viscous fluid. Royal Soc Aerodyn Dep Natl Phys Lab. 1925;225:626–35. https://doi.org/10.1098/rsta.1926.0003.
12. Riley N. The heat transfer from a rotating disk. J Mech Appl Math. 1964;17(3):331–49. https://doi.org/10.1093/qjmam/17.3.331.
13. Smyth R, Zurita P. Heat transfer at the outer surface of a rotating cylinder in the presence of axial flows. WIT Trans Eng Sci. 1994;5:8. https://doi.org/10.2495/HT940171.
14. Pekdemir T, Davies TW. Mass transfer from rotating circular cylinders in a submerged slot jet of air. Int J Heat Mass Transf. 1998;41:3441–50. https://doi.org/10.1016/S0017-9310(98)00056-8.
15. Zoueshtiagh F, Ali R, Colley AJ, Thomas PJ. Laminar-turbulent boundary-layer transition over a rough rotating disk. Phys Fluid J. 2003;15:2441. https://doi.org/10.1063/1.1586916.
16. Seghir-Ouali S, Saury D, Harmand S, Phillipart O, Laloy D. Convective heat transfer inside a rotating cylinder with an axial air flow. Int J Therm Sci. 2006;45:1166–78. https://doi.org/10.1016/j.ijthermalsci.2006.01.017.
17. Pavlovich Moshkin N, Sompong J. Numerical simulation of heat transfer and fluid flow over two rotating circular cylinders at low Reynolds number. Heat Transf Asian Res Cospons Soc Chem Eng Jpn Heat Transf Div ASME. 2010;39:246–61. https://doi.org/10.1002/htj.20293.
18. Fénot M, Bertin Y, Dorignac E, Lalizel G. A review of heat transfer between concentric rotating cylinders with or without axial flow. Int J Therm Sci. 2011;50:1138–55. https://doi.org/10.1016/j.ijthermalsci.2011.02.013.
19. Mahmoodi M, Sebdani SM. Natural convection in a square cavity containing a nanofluid and an adiabatic square block at the center. Superlattices Microstruct. 2012;52:261–75. https://doi.org/10.1016/j.spmi.2012.05.007.
20. Sharma V, Dhiman AK. Heat transfer from a rotating circular cylinder in the steady regime: effect of Prandtl number. Therm Sci. 2012;16(1):79–91. https://doi.org/10.2298/TSCI100914057S.
21. Roslan R, Saleh H, Hashim I. Effect of rotating cylinder on heat transfer in a square enclosure filled with nanofluids. Int J Heat Mass Transf. 2012;55:7247–56. https://doi.org/10.1016/j.ijheatmasstransfer.2012.07.051.
22. Fang T, Tao H. Unsteady viscous flow over a rotating stretchable disk with deceleration. Commun Nonlinear Sci Numer Simul. 2012;17:5064–72. https://doi.org/10.1016/j.cnsns.2012.04.017.
23. Harmand S, Pellé J, Poncet S, Shevchuk IV. Review of fluid flow and convective heat transfer within rotating disk cavities with impinging jet. Int J Therm Sci. 2013;67:1–30. https://doi.org/10.1016/j.ijthermalsci.2012.11.009.
24. Chatterjee D, et al. Mixed convective transport in a lid-driven cavity containing a nanofluid and a rotating circular cylinder at the center. Int Commun Heat Mass Transf. 2014;56:71–8. https://doi.org/10.1016/j.icheatmasstransfer.2014.06.002.
25. Bouakkaz R, Talbim K, Ouazzazi M, Khelili Y, Salhi F. Effect of rotation rates on the laminar flow and heat transfer past a circular cylinder. Braz J Chem Eng. 2015;32:519–29. https://doi.org/10.1590/0104-6632.20150322s00002539.
26. Capone A, Klein C, Di Felice F, Miozzi M. Phenomenology of a flow around a circular cylinder at sub-critical and critical

Reynolds numbers. Phys Fluids. 2016;28:074101. https://doi.org/10.1063/1.4954655.
27. Kareem AK, Gao S. Mixed convection heat transfer of turbulent flow in a three- dimensional lid-driven cavity with a rotating cylinder. Int J Heat Mass Transf. 2017;112:185–200. https://doi.org/10.1016/j.ijheatmasstransfer.2017.04.118.
28. Turkyilmazoglu M. Fluid flow and heat transfer over a rotating and vertically moving disk. Phys Fluids. 2018;30:063605. https://doi.org/10.1063/1.5037460.
29. Barati E, et al. Effect of rotational direction of circular cylinder for mixed convection at subcritical Reynolds number. In: The 27th annual international conference of iranian society of mechanical engineers, Tehran, 2019.
30. Kumar D, Sahu AK. Forced convection heat transfer from a rotating elliptic cylinder in the laminar flow regime. In: The 25th national and 3rd international heat and mass transfer conference, Roorkee, 2019.
31. Chen S-X, Zhang J-Z. Effects of the rotation number on flow and heat transfer in contra-rotating disk cavity with superposed flow. Adv Mech Eng. 2019. https://doi.org/10.1177/1687814019881041.
32. Zafar F, Alam MM. Mixed convection heat transfer from a circular cylinder submerged in wake. Int J Mech Sci. 2020. https://doi.org/10.1016/j.ijmecsci.2020.105733.
33. Safarzadeh S, Rahimi AB. Convective heat transfer and flow phenomena from a rotating sphere in porous media. Sci Iran Trans B Mech Eng. 2022;29:588–96. https://doi.org/10.24200/SCI.2021.53800.3422.
34. Chen Z. Mixed convection between rotating sphere and concentric cubical enclosure. Phys Fluids. 2021;33:013605. https://doi.org/10.1063/5.0039830.
35. Pantokratoras A. Forced convection heat transfer from a heated rotating sphere in laminar flow revisited. Int J Thermofluids. 2021. https://doi.org/10.1016/j.ijft.2021.100090.
36. Feng Z-G. Direct numerical simulation of forced convective heat transfer from a heated rotating sphere in laminar flows. J Heat Transf. 2014. https://doi.org/10.1115/1.4026307.
37. Jabbar MY, Hamzah HK, Ali FH, Ahmed SY, Ismael MA. Thermal analysis of nanofluid saturated in inclined porous cavity cooled by rotating active cylinder subjected to convective condition. J Therm Anal Calorim. 2021;144:1299–323. https://doi.org/10.1007/s10973-020-09668-x.
38. Davoodabadi S, Oztop HF. Natural convection in a rectangular tall cavity in the presence of an oscillating and rotating cylinder. Colloids Surf A Physicochem Eng Asp. 2022;647:129027. https://doi.org/10.1016/j.colsurfa.2022.129027.
39. White FM. Fluid mechanics. Boston: McGraw-Hill; 1999.
40. Versteeg HK, Malalasekera W. An introduction to computational fluid dynamics: the finite method. London: Pearson Education; 2007.
41. Kareem AK, Gao S, Ahmed AQ. Unsteady simulations of mixed convection heat transfer in a 3D closed lid-driven cavity'. Int J Heat Mass Transf. 2016;100:121–30. https://doi.org/10.1016/j.ijheatmasstransfer.2016.04.073.
42. Huang P, Bardina J, Coakley T. Turbulence modeling validation, testing, and development. Washington, D.C.: NASA Technical Memorandum; 1997.
43. Nicoud F, Ducros F. Subgrid-scale stress modelling based on the square of the velocity gradient tensor. Flow Turbul Combust. 1999;62:183–200. https://doi.org/10.1023/A:1009995426001.
44. Ben-Cheikh N, Hammami F, Campo A, Ben-Beya B. A dynamic sub-grid scale model for large eddy simulation of turbulent flows in a lid-driven cubical cavity. Comptes Rendus Méc. 2012;340:721–30. https://doi.org/10.1016/j.crme.2012.10.001.
45. ANSYS Fluent Tutorial Guide, ANSYS, Inc., 2017.